

GALAXY NUMBER COUNTS IN THE SUBARU DEEP FIELD: MULTI-BAND ANALYSIS IN A HIERARCHICAL GALAXY FORMATION MODEL

MASAHIRO NAGASHIMA,¹ YUZURU YOSHII,^{2,3} TOMONORI TOTANI,^{1,4} AND NAOTERU GOUDA¹

masa@th.nao.ac.jp

To appear in ApJ

ABSTRACT

Number counts of galaxies are re-analyzed using a semi-analytic model (SAM) of galaxy formation based on the hierarchical clustering scenario. Faint galaxies in the Subaru Deep Field (SDF, near-infrared J and K') and the Hubble Deep Field (HDF, ultraviolet/optical U , B , V , and I) are compared with our model galaxies. We have determined the astrophysical parameters in the SAM that reproduce observations of nearby galaxies, and used them to predict the number counts and redshifts of faint galaxies for three cosmological models, the standard cold dark matter (CDM) universe, a low-density flat universe with nonzero cosmological constant, and a low-density open universe with zero cosmological constant. The novelty of our SAM analysis is the inclusion of selection effects arising from the cosmological dimming of surface brightness of high-redshift galaxies, and from the absorption of visible light by internal dust and intergalactic H I clouds. As was found in our previous work, in which the ultraviolet/optical HDF galaxies were compared with our model galaxies, we find that our SAM reproduces counts of near-infrared SDF galaxies in a low-density universe either with or without a cosmological constant, and that the standard CDM universe is *not* preferred, as suggested by other recent studies. Moreover, we find that simple prescriptions for (1) the timescale of star formation being proportional to the dynamical time scale of the formation of galactic disks, (2) the size of galactic disks being rotationally supported with the same specific angular momentum as that of surrounding dark halo, and (3) the dust optical depth being proportional to the metallicity of cold gas, cannot completely explain all of observed data. Improved prescriptions incorporating mild redshift-dependence for those are suggested from our SAM analysis.

Subject headings: cosmology: theory – galaxies: evolution – galaxies: formation – large-scale structure of universe

1. INTRODUCTION

It is well known that the number of faint galaxies in a given area of sky can constrain cosmological parameters, because it depends on the geometry of the Universe (e.g., Peebles 1993). Many efforts have been devoted to this subject using traditional galaxy evolution models assuming monolithic collapse, such as the wind model for elliptical galaxies and the infall model for spiral galaxies (e.g., Yoshii & Takahara 1988). These models are in fact able to reproduce many of the observed properties of nearby galaxies, and provide a useful theoretical tool for understanding their evolution (Arimoto & Yoshii 1986, 1987; Arimoto, Yoshii & Takahara 1991).

In the analyses of galaxy counts from traditional approaches, it has been found that the Einstein-de Sitter (EdS) universe, a representation of the standard cold dark matter (CDM) universe, is not reconcilable with the observed high counts of faint galaxies, and that a low-density universe is preferred (Yoshii & Takahara 1988; Yoshii & Peterson 1991, 1995; Yoshii 1993). Recently, Totani & Yoshii (2000) and Totani et al. (2001a) compared their predictions against the observed number counts to the faint limits in the Hubble Deep Field (HDF; Williams et al. 1996) and in the Subaru Deep Field (SDF; Maihara et al. 2001), taking into account various selection effects and allowing for the possibility of number evolution of galaxies in a phenomenological way. Note that the SDF counts are now the deepest near-infrared ones with the 5σ limiting magnitude of $K = 23.5$ in to-

tal magnitude. They confirmed that the EdS universe cannot reproduce the observed high counts. However, in their best-fit models, the merger rates of HDF and SDF galaxies are a little different. A mild merger rate is needed to reproduce the counts in the HDF, while a negligible rate was necessary for the SDF. It should be noted that the photometric passbands for the two applications are different; ultraviolet/optical for the HDF and near-infrared for the SDF. They suggested that the difference of the merger rate might be originated by morphology-dependent number evolution because late-type galaxies are mainly seen in shorter wavelength such as B -band and early-type galaxies are seen in longer wavelength such as K -band. In any case, it should be explained why the merger rate depends on the observed wavelength in order to obtain a better understanding of the galaxy formation process.

On the other hand, in the study of formation of large-scale structure in the universe, both theory and observation suggest that gravitationally bound objects, such as galaxy clusters, are formed through continuous mergers of dark halos with an initial density fluctuation spectrum predicted by the CDM models. Based on this scenario of *hierarchical clustering*, the so-called semi-analytic models (SAMs) of galaxy formation have been developed by a number of authors (Kauffmann, White & Guiderdoni 1993; Cole et al. 1994, 2000; Somerville & Primack 1999; Nagashima et al. 2001, hereafter NTGY). SAMs successfully reproduced a variety of observed features of local galaxies, such as their luminosity function, color distribution,

¹ National Astronomical Observatory, Mitaka, Tokyo 181-8588, Japan

² Institute of Astronomy, Graduate School of Science, The University of Tokyo, 2-21-1 Osawa, Mitaka, Tokyo 181-8588, Japan

³ Research Center for the Early Universe, Graduate School of Science, The University of Tokyo, 7-3-1 Hongo, Bunkyo-ku, Tokyo 113-0033, Japan

⁴ Peyton Hall, Princeton University, Princeton, NJ08544-1001, USA

and so on.

Faint galaxy number counts have also been analyzed using SAMs (Cole et al. 1994; Kauffmann, Guiderdoni & White 1994; Heyl et al. 1995; Baugh, Cole & Frenk 1996). These studies showed that predicted number counts in the EdS universe agree with the observed counts. Their results, however, contradict analyses carried out with traditional galaxy evolution models. Recently, this contradiction was resolved by NTGY, in which their SAM is compared with the galaxy counts in the HDF. They found, by matching properties of model galaxies with observation especially in local luminosity functions and cold gas mass fraction, that normalization of model parameters, related to combinations of physical processes such as star formation (SF) and supernova (SN) feedback, is very important, and that accounting for selection effects caused by cosmological dimming of surface brightness and absorption of emitted light by internal dust and intergalactic H I clouds is crucial in the analysis of galaxy counts, as shown by Totani & Yoshii (2000). It should be noted that recent analysis by Lanzetta et al. (2001) also clarify the importance of the selection effects caused by the cosmological dimming of surface brightness in the observational point of view. They introduced the star formation rate intensity distribution function, which was derived from the ultraviolet luminosity density for the HDF galaxies, at several redshifts and found that at high redshift significant fraction of ultraviolet luminosity density must be missed due to the cosmological dimming of surface brightness.

The purpose of this paper is to examine whether our SAM can *simultaneously* reproduce both the ultraviolet/optical and near-infrared galaxy counts in the HDF and in the SDF. Because the luminosity of galaxies in different passbands reflects the influence of different stellar populations, the subject of multi-band number counts provides a strong constraint on galaxy formation. In this paper, using selection criteria for SDF galaxies based on Totani et al. (2001a), we compare our SAM prediction of galaxy counts with the observed counts in the SDF.

This paper is outlined as follows. In §2 we briefly describe our SAM, which is almost the same as our previous models (NTGY). In §3 we constrain the astrophysical parameters in our SAM analysis using local observations. In §4 we compare theoretical number counts of faint galaxies with the HDF and SDF data, and in §5 we discuss the range of uncertainties in our calculations of galaxy number counts. In §6 we provide a summary and discussion.

2. MODEL

The galaxy formation scenario that we model is as follows. In the CDM universe, dark matter halos cluster gravitationally, and merge in a manner that depends on the adopted power spectrum of the initial density fluctuations. In each of the merged dark halos, radiative gas cooling, star formation, and gas reheating by supernovae occur. The cooled dense gas and stars constitute *galaxies*. These galaxies sometimes merge together in a common dark halo, and more massive galaxies form. Repeating these processes, galaxies form and evolve to the present epoch.

The SAM analysis we perform obtains essentially the same results of our previous SAM analyses, with minor differences in a number of details. In this section we briefly describe our model. Details of the model we employ are described in NTGY, except for a few differences, which are explicitly mentioned below.

2.1. Scheme of Galaxy Formation

The merging histories of dark halos are realized by a Monte Carlo method proposed by Somerville & Kolatt (1999), based on the extended Press-Schechter formalism (Bond et al. 1991; Bower 1991; Lacey & Cole 1993). This formalism is an extension of the Press-Schechter formalism (Press & Schechter 1974), which gives us the mass function of dark halos, $n(M)dM$, to estimate the mass function of progenitor halos with mass M_1 at a redshift $z_0 + \Delta z$ of a single dark halo with mass M_0 collapsing at a redshift z_0 , $n(M_1; z_0 + \Delta z | M_0; z_0)dM_1$. Dark halos with circular velocity $V_{\text{circ}} \geq 40 \text{ km s}^{-1}$ are regarded as isolated halos, and otherwise regarded as diffuse accreted matter. The mean density in dark halos is assumed to be proportional to the cosmic mean density at the collapsing epoch using a spherically symmetric collapse model (Tomita 1969; Gunn & Gott 1972). Each collapsing dark halo contains baryonic matter with a mass fraction Ω_b/Ω_0 , where Ω_0 and Ω_b are the parameters of total and baryon mass densities relative to the critical cosmic mass density. We adopt a value of $\Omega_b = 0.015h^{-2}$ given by Suzuki, Yoshii & Beers (2000) in which they estimated the value from the primordial lithium abundance, where h is the Hubble parameter, $h \equiv H_0/100 \text{ km s}^{-1} \text{ Mpc}^{-1}$. Note that a recent measurement of the anisotropy of the cosmic microwave background by the BOOMERANG project suggests a slight higher value, $\Omega_b \simeq 0.02h^{-2}$ (Netterfield et al. 2001). The effect of changing Ω_b has already been investigated by Cole et al. (2000) and they showed that this mainly affects the value of the invisible stellar mass fraction such as brown dwarfs parametrized by Υ (see the next subsection). We also checked whether our results are changed or not in the case of $\Omega_b \sim 0.04$ and found that this does not affect them. The baryonic matter consists of diffuse hot gas, dense cold gas, and stars.

When a halo collapses, the hot gas is shock-heated to the virial temperature of the halo with an isothermal density profile. A part of the hot gas cools and accretes to disk of a galaxy until the subsequent collapse of the dark halos. The amount of the cold gas involved is calculated by using metallicity-dependent cooling functions provided by Sutherland & Dopita (1993). The difference of cooling rates between the primordial and metal-polluted gases is prominent at $T \sim 10^6 \text{ K}$ due to line-cooling of metals. The cooling is, however, very efficient in dark halos with a virial temperature of $T \sim 10^6 \text{ K}$ even in the case of the primordial gas, so the metallicity dependence of cooling rate only slightly affects our results. In order to avoid the formation of unphysically large galaxies, the cooling process is applied only to halos with $V_{\text{circ}} < 500 \text{ km s}^{-1}$ in the standard CDM and 400 km s^{-1} in low-density universes according to some previous SAMs. This handling would be needed because the simple isothermal distribution forms so-called “monster galaxies” due to the too efficient cooling at the center of halos. While this problem will probably be solved by adopting another isothermal distribution with central core (Cole et al. 2000), we take the above simple approach because this does not cause any serious problems in estimating galaxy counts.

Stars in the disk are formed from the cold gas. The SF rate (SFR) \dot{M}_* is given by the cold gas mass M_{cold} and a SF timescale τ_* as $\dot{M}_* = M_{\text{cold}}/\tau_*$. We use two SF models. One model adopts constant star formation (CSF), in which τ_* is a constant against redshift; the other adopts dynamical star formation (DSF), in which τ_* is proportional to the dynamical timescale of the halo, which allows for the possibility that the SF efficiency is variable with redshift. We then express the SF

timescale as

$$\tau_* = \begin{cases} \tau_*^0 \left(\frac{V_{\text{circ}}}{300 \text{ km s}^{-1}} \right)^{\alpha_*} & \text{(CSF),} \\ \tau_*^0 \left(\frac{V_{\text{circ}}}{300 \text{ km s}^{-1}} \right)^{\alpha_*} \left[\frac{\tau_{\text{dyn}}(z)}{\tau_{\text{dyn}}(0)} \right] (1+z)^\sigma & \text{(DSF),} \end{cases} \quad (1)$$

where τ_*^0 , α_* and σ are free parameters. The former two parameters are chosen so as to match the fraction of cold gas mass with the observed fraction (see next section). While, of course, some fraction of cold gas might not be seen, we adopt the gas mass fraction to constrain the SF-related parameters according to Cole et al. (2000). If much of this cold gas would be hidden, τ_*^0 should be longer than our value. Note that in our previous paper (NTGY) we used DSF only in the case of $\sigma = 0$. In Figure 1 we show the timescales for CSF (dot-dashed line) and DSF with $\sigma = 0$ (solid line) and $\sigma = 1$ (dashed line) in a Λ -dominated flat universe. Because objects which collapsed at higher redshift have higher density, the dynamical timescale τ_{dyn} is shorter at higher redshift. Thus, the DSF scenario with smaller σ converts the cold gas into stars more rapidly than the CSF. In this paper we examine not only the CSF and $\sigma = 0$ DSF models but also the DSF model with $\sigma = 1$ as an intermediate case.

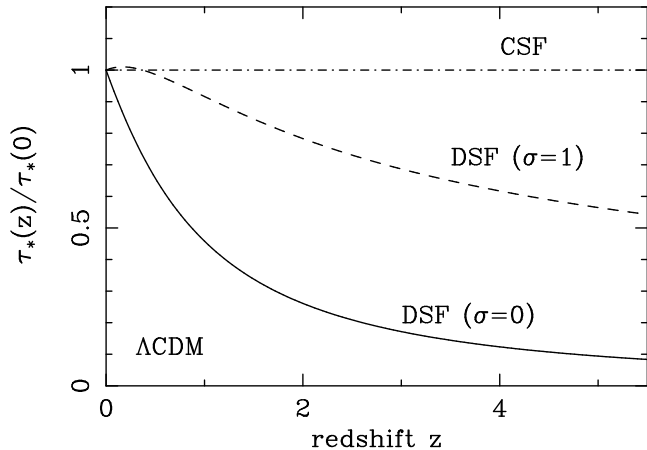


FIG. 1.— Star formation timescales τ_* as a function of redshift z in a Λ -dominated flat CDM model. The timescale is normalized by that evaluated at present. The dot-dashed line denotes the constant SF model (CSF). The solid line denotes the dynamical star formation model (DSF) with $\sigma = 0$ for which the timescale is proportional to the dynamical timescale of disk. The dashed line denotes the DSF with $\sigma = 1$ as an intermediate case between CSF and DSF with $\sigma = 0$.

Massive stars explode as Type II supernovae (SNe) and heat up the surrounding cold gas. This SN feedback reheats the cold gas at a rate of $\dot{M}_{\text{reheat}} = M_{\text{cold}}/\tau_{\text{reheat}}$, where the timescale of reheating is given by

$$\tau_{\text{reheat}} = \left(\frac{V_{\text{circ}}}{V_{\text{hot}}} \right)^{\alpha_{\text{hot}}} \tau_*. \quad (2)$$

The free parameters V_{hot} and α_{hot} are determined by matching the local luminosity function of galaxies with observations.

With the parameters \dot{M}_* and \dot{M}_{reheat} thus determined, we obtain the masses of hot gas, cold gas, and disk stars as a function of time during the evolution of galaxies. Chemical enrichment is also taken into account, adopting *heavy-element yield* of $y = 0.038 = 2Z_\odot$, but changing this value of y has a minimal effect on the results described below.

When two or more progenitor halos have merged, the newly formed larger halo should contain at least two or more galaxies which had originally resided in the individual progenitor halos. By definition, we identify the central galaxy in the new common halo with the central galaxy contained in the most massive one of the progenitor halos. Other galaxies are regarded as satellite galaxies. These satellites merge by either dynamical friction or random collision. The timescale of merging by dynamical friction τ_{fric} is given by Binney & Tremaine (1987), which is estimated from the baryonic mass of satellite. When the time elapsed after merging of progenitor halos exceeds τ_{fric} , a satellite galaxy in the common halo is accreted to the central galaxy. On the other hand, the mean free timescale of random collision τ_{coll} is given by Makino & Hut (1997). With a probability $\Delta t/\tau_{\text{coll}}$, where Δt is the time step corresponding to the redshift interval Δz of merger tree of dark halos, a satellite galaxy merges with another satellite picked out randomly.

Consider the case when two galaxies of masses m_1 and $m_2 (> m_1)$ merge together. If the mass ratio $f = m_1/m_2$ is larger than a certain critical value of f_{bulge} , we assume that a starburst occurs and that all of the cold gas turns into stars and hot gas, which fills the resulting halo, and all of the stars populate the bulge of a new galaxy. On the other hand, if $f < f_{\text{bulge}}$, no starburst occurs, and a smaller galaxy is simply absorbed into the disk of a larger galaxy. This division into major and minor modes is only for simplicity and we adopt $f_{\text{bulge}} = 0.1$ as a standard value. As shown in Figure 13, the dependence of total counts on f_{bulge} is negligible (see §5.4). Although there is a model to treat continuous burst activity, say, as a function of the mass ratio f (Somerville, Primack & Faber 2001), we adopt the above simple division because of the negligible dependence on f_{bulge} .

2.2. Photometric Properties of Galaxies

The above processes are repeated until the output redshift and then the SF history of each galaxy is obtained. For the purpose of comparison with observation, we use a stellar population synthesis approach, from which the luminosities and colors of model galaxies are calculated. Given the SFR as a function of time or redshift, the absolute luminosity and colors of individual galaxies are calculated using a population synthesis code by Kodama & Arimoto (1997). The stellar metallicity grids in the code cover a range from $Z_* = 0.0001$ to 0.05. Note that we now define the metallicity as mass fraction of metals, for example, the solar metallicity is 0.019. The initial stellar mass function (IMF) that we adopt is the power-law IMF of Salpeter form, with lower and upper mass limits of $0.1M_\odot$ and $60M_\odot$, respectively. Then, following Cole et al. (1994), we introduce a parameter defined as $\Upsilon = (M_{\text{lum}} + M_{\text{BD}})/M_{\text{lum}}$, where M_{lum} is the total mass of luminous stars with $m \geq 0.1M_\odot$ and M_{BD} is that of invisible brown dwarfs.

Our model of estimating the optical depth of internal dust has been improved over that adopted by NTGY. We take the usual assumption that the abundance of dust is proportional to the metallicity of cold gas, and that the optical depth is proportional to the column density of metallicity. Then the optical depth τ is given by

$$\tau \propto \frac{M_{\text{cold}} Z_{\text{cold}}}{r_e^2} (1+z)^{-\gamma}, \quad (3)$$

where r_e is the effective radius of the galactic disk, described in the next subsection. The proportionality constant is determined by matching the extinction, $A_V \approx 0.2$, for galaxies typical of the

Milky Way, assuming the slab dust model according to our previous paper (NTGY) and Somerville & Primack (1999). We adjust the high redshift properties of dust-to-metal ratio and dust clumpiness by changing γ . As a standard model, we simply adopt $\gamma = 0$. It will be also investigated in §5.3 how the galaxy counts are affected by γ .

For some classes of galaxies, the screen dust model has been suggested to be a good approximation, rather than the slab dust model. For example, some galaxies such as nearby starburst galaxies and hyper extremely red objects (HEROs) are very red and therefore their dust distribution should be approximated by the screen model (Totani et al. 2001b). Besides recent analysis of source counts in far-infrared and submillimeter wavelengths also favors the screen dust model (Totani & Takeuchi 2002). In this paper, however, we adopt the slab model as a standard one because main contribution in UV/optical and near-infrared passbands is considered to be galaxies which are not heavily extinguished under modest star formation activity. Of course, even for these normal galaxies the screen dust model might be a good approximation. Therefore we will check the screen dust model in §5.3. While we check only these two models, the uncertainty caused by the dust model would be clarified by checking these models and by varying γ .

Emitted light from distant galaxies is absorbed by Lyman lines and Lyman continuum in intervening intergalactic H I clouds. We used an optical depth calculated by Yoshii & Peterson (1994) to account for this.

We classify galaxies into different morphological types according to the B -band bulge-to-disk luminosity ratio B/D . In this paper, following Simien & de Vaucouleurs (1986), galaxies with $B/D \geq 1.52$, $0.68 \leq B/D < 1.52$, and $B/D < 0.68$ are classified as ellipticals, S0s, and spirals, respectively. Kauffmann, White & Guiderdoni (1993) and Baugh, Cole & Frenk (1996) showed that this method of type classification reproduces the observed type mix well.

We then assess whether the surface brightnesses of model galaxies are above the detection thresholds of the SDF and HDF observations. The selection effects in our SAM analysis are evaluated as follows. Using the intrinsic size of model galaxies, described in the next subsection, their surface brightness profiles in the observers frame are given by a convolution of the luminosity profile with a Gaussian point-spread function. Here we assume an exponential profile for spiral galaxies, and a de Vaucouleurs profile for elliptical and lenticular galaxies. We note that model galaxies with surface brightness higher than the threshold S_{th} , and isophotal areas larger than the minimum area A_{th} are actually detected as galaxies (Yoshii 1993). Following Totani & Yoshii (2000) and Totani et al. (2001a), we adopt $S_{\text{th}} = 25.59 \text{ mag arcsec}^{-2}$ in K' , $S_{\text{th}} = 24.10 \text{ mag arcsec}^{-2}$ in J , and $A_{\text{th}} = 0.24 \text{ arcsec}^2$ for the SDF galaxies, and $S_{\text{th}} = 27.5 \text{ mag arcsec}^{-2}$ in V_{606} , $S_{\text{th}} = 27.0 \text{ mag arcsec}^{-2}$ in I_{814} , U_{300} and B_{450} , and $A_{\text{th}} = 0.04 \text{ arcsec}^2$ for the HDF galaxies.

For the SDF galaxies, we also take into account the detection probability, that is, completeness. Noise and statistical fluctuations in the data prevent complete source detections at any specified limits of surface brightness and size. Totani et al. (2001a) found that the dispersion of observed isophotal area around its true value can be fitted by

$$\sigma_A(m, d_{\text{ob}}) = c(A_1 - A_2)^{1/2} d_{\text{ob}}, \quad (4)$$

where m is the total magnitude of an object, d_{ob} is the FWHM size, and A_1 and A_2 are the isophotal areas corresponding to

the isophotal level 0.8 and 1.2 times brighter than S_{th} , respectively. Assuming a Gaussian distribution of observed isophotal area with this dispersion, we obtain the probability that the observed isophotal area is larger than the threshold value A_{th} . Additional details of these selection effects are described in Totani & Yoshii (2000) and Totani et al. (2001a).

2.3. Galaxy Size

We assume that the size of spiral galaxies is determined by a radius at which the gas is supported by rotation, under the conservation of specific angular momentum of hot gas that cools and contracts. We also assume that the initial specific angular momentum of the gas is the same as that of the host dark halo. Acquisition of the angular momentum of dark halos is determined by the tidal torques in the initial density fluctuation field (White 1984; Catelan & Theuns 1996a,b; Nagashima & Gouda 1997). The distribution of the dimensionless spin parameter λ_H is well approximated by a log-normal distribution (Mo, Mao & White 1998),

$$p(\lambda_H) d\lambda_H = \frac{1}{\sqrt{2\pi}\sigma_\lambda} \exp\left[-\frac{(\ln \lambda_H - \ln \bar{\lambda})^2}{2\sigma_\lambda^2}\right] d\ln \lambda_H, \quad (5)$$

where $\bar{\lambda}$ is the mean value of spin parameter and σ_λ is its logarithmic variance. We adopt $\bar{\lambda} = 0.05$ and $\sigma_\lambda = 0.5$. (Note that in our previous paper we adopted $\lambda_H = 0.05$ for all spirals.) If the specific angular momentum is conserved, the effective radius r_e of a presently observed galaxy at $z = 0$ is related to the initial radius r_i of the progenitor gas sphere via $r_e = (1.68/\sqrt{2})\lambda_H r_i$ (Fall 1979; Fall & Efstathiou 1980; Fall 1983). The initial radius r_i is set to be the smaller one between the virial radius of the host halo and the cooling radius. A disk of a galaxy grows due to cooling and accretion of hot gas from more distant envelope of its host halo. In our model, when the estimated radius by the above equation becomes larger than that in the previous step, the radius grows to the new larger value in the next step.

Size estimation of high-redshift spiral galaxies, however, carries uncertainties because of the large dispersion in their observed size distribution. Allowing for the possibility that the conservation of angular momentum is not complete, we generalize this size estimation by introducing a simple redshift dependence,

$$r_e = \frac{1.68}{\sqrt{2}} \lambda_H r_i (1+z)^\rho, \quad (6)$$

where ρ is a free parameter; we simply use $\rho = 0$ as a reference value in this paper. Results for other values of ρ will be given in §5. The effect of changing ρ emerges in the selection effects due to the cosmological dimming of surface brightness and in the dust extinction because the dust column density also changes with galaxy size.

Figure 2 shows the effective disk radii of spiral galaxies at $z = 0$ as a function of their luminosity for the models of SC (thick solid line), OC (dashed line), and LC (dot-dashed line). The adopted parameters in these models are tabulated in Table 1. All the models well reproduce the observed disk size-magnitude relation (thin solid line) compiled by Totani & Yoshii (2000) based on the data taken from Impey et al. (1996). The redshift dependence of such relation through changing ρ in equation 6 will be discussed in §5.

The sizes of early-type galaxies, which likely form from galaxy mergers, are determined by the virial radius of the baryonic component. When a major merger of galaxies occurs, the

merged system consisting of stars and cold gas initially virializes to satisfy

$$V_{\text{circ}}^2 = \frac{G(M_* + M_{\text{cold}})}{r_i}. \quad (7)$$

In this paper we take into account the dynamical response to the “shallowing” of the gravitational potential due to the mass loss caused by the SN feedback. Then, after the initial virialization, the system expands while losing the cold gas, with the adiabatic invariant $(M_* + M_{\text{cold}})r$ kept constant (e.g., Yoshii & Arimoto 1987). Then the final radius of the system, consisting only of stars after the loss of the cold gas, is given by

$$r_f = \frac{M_{*,i} + M_{\text{cold}}}{M_{*,f}} r_i, \quad (8)$$

where $M_{*,i}$ and $M_{*,f}$ are the total masses of stars in the system before and after the mass loss, respectively. The effect of the dynamical response is most prominent for dwarf galaxies of lower circular velocity, and can explain the properties of local dwarf ellipticals, which will be presented in a separate paper. However, this effect has only a minor impact on our predicted galaxy number counts, because luminous galaxies of larger circular velocity are the main contributors to galaxy number counts at the faint limits under consideration. In order to match with the observed effective radius, we here introduce a scaling parameter, f_b , such that $r_e = f_b r_f$. The adopted values of f_b for SC, OC, and LC are tabulated in Table 1.

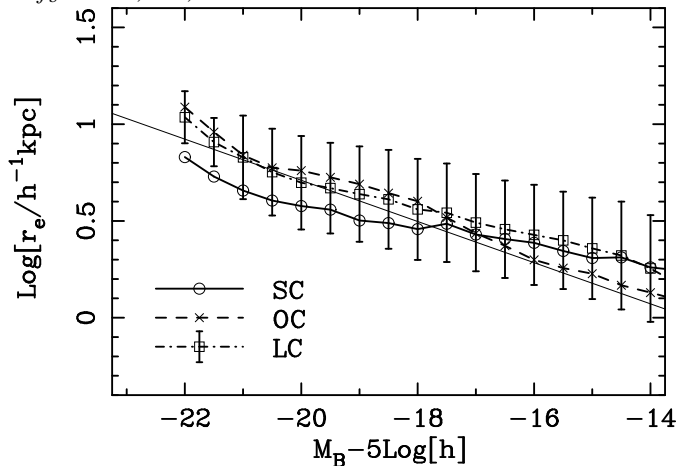


FIG. 2.— Galaxy sizes. The thick solid line connecting open circles, the dashed line connecting crosses, and the dot-dashed line connecting open squares show theoretical results for effective radii of late-type galaxies in the SC, OC, and LC models, respectively. We show 1σ scatter in the LC model by error bars. Similar scatter in other models are not shown. The thin line shows the observed best-fit relation given by Totani & Yoshii (2000) for spiral galaxies, based on the data taken from Impey et al. (1996).

3. PARAMETER SETTINGS

We normalize the model parameters so as to agree with various local observations. As shown in NTGY, this normalization procedure is an essential ingredient in the analysis of galaxy counts.

The cosmological parameters (Ω_0 , Ω_Λ , h , σ_8) adopted in this paper are tabulated in Table 1. For all the models (SC, OC, and LC), the baryon density parameter $\Omega_b = 0.015h^{-2}$ is used in common. For OC and LC the value of $\sigma_8 = 1$ is determined from observed cluster abundances (Eke, Cole & Frenk 1996).

The astrophysical parameters (V_{hot} , α_{hot} , τ_*^0 , α_* , f_b , f_{bulge} , Υ) are constrained from local observations as discussed below.

The adopted values are almost the same as in our previous paper. Slight differences have resulted from modifications to the model, such as the improved scheme of dust extinction. In this paper we only show the result of CSF (equation 1) as a standard, and other parameters used in common, including $\gamma = 0$ (equation 3), $\rho = 0$ (equation 6), and $(\bar{\lambda}, \sigma_\lambda) = (0.05, 0.5)$ (equation 5).

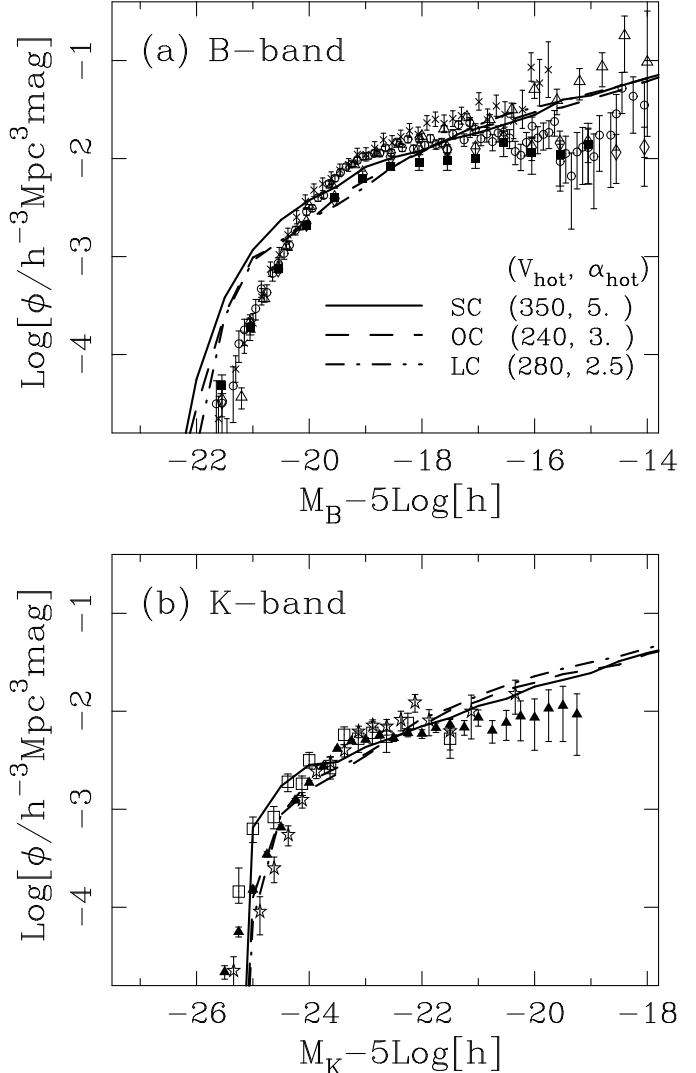


FIG. 3.— Local luminosity functions in the (a) B band and (b) K band. The solid, dashed, and dot-dashed lines indicate the SC, OC, and LC models, respectively. Symbols with error bars in (a) indicate the observational data from APM (Loveday et al. 1992, *filled squares*), ESP (Zucca et al. 1997, *open triangles*), Durham/UKST (Ratcliffe et al. 1998, *open diamonds*), 2dF (Folkes et al. 1999, *open circles*), and SDSS (Blanton et al. 2000, *crosses*). Note that the SDSS luminosity function shown here is that with the same detection limit as employed in the 2dF survey. Symbols in (b) indicate the data from Mobasher et al. (1993, *open squares*), Gardner et al. (1997, *open stars*), and 2MASS (Cole et al. 2000, *filled triangles*).

First, the SN feedback-related parameters (V_{hot} , α_{hot}) and the mass fraction Υ of invisible stars are almost uniquely determined if their values are chosen so as to reproduce the local luminosity function. Figure 3 shows theoretical results for the models of SC (thick solid line), OC (dashed line), and LC (dot-dashed line), which are tabulated in Table 1. Symbols with error bars indicate observational results from the B -band redshift surveys, such as APM (Loveday et al. 1992), ESP (Zucca et al. 1997), Durham/UKST (Ratcliffe et al. 1998), 2dF (Folkes et al. 1999) and SDSS (Blanton et al. 2001), and from the K -

band redshift surveys (Mobasher et al. 1993; Gardner et al. 1997; 2MASS, Cole et al. 2001). As done in NTGY, we regard the APM result as a standard one. This gives somewhat less normalization of luminosity function compared with other surveys, probably because of its worse completeness compared to the other recent surveys. Nevertheless, in this paper, we determine the SN feedback-related parameters in the above way because the dependence of these parameters on galaxy counts has been already investigated by NTGY and then because it has been found that the shape of counts is not significantly affected. We checked that the shape of the counts in the K' -band are also not affected by changing the luminosity function significantly.

Next, the SFR-related parameters (τ_*^0 , α_*) are determined by using the cold gas mass fraction in late-type galaxies. The gas fraction depends on both the SN feedback-related parameters and on the SFR-related ones. The former parameters determine the gas fraction expelled from galaxies and the latter ones the gas fraction that is converted into stars. Therefore, in advance of determining the SFR-related parameters, the SN feedback-related parameters must be determined by matching the local luminosity function.

Figure 4 shows the ratio of cold gas mass relative to B -band luminosity of spiral galaxies as a function of their luminosity. Theoretical results are shown for the models of SC (thick solid line), OC (dashed line), and LC (dot-dashed line). We here assume that 75% of the cold gas in these models is comprised of hydrogen, i.e., $M_{\text{HI}} = 0.75M_{\text{cold}}$. HI data, taken from Huchtmeier & Richter (1988), are shown by open squares with error bars. Since their data do not include the fraction of H_2 molecules, the observational result should be regarded as providing a lower limit of the cold gas mass fraction.

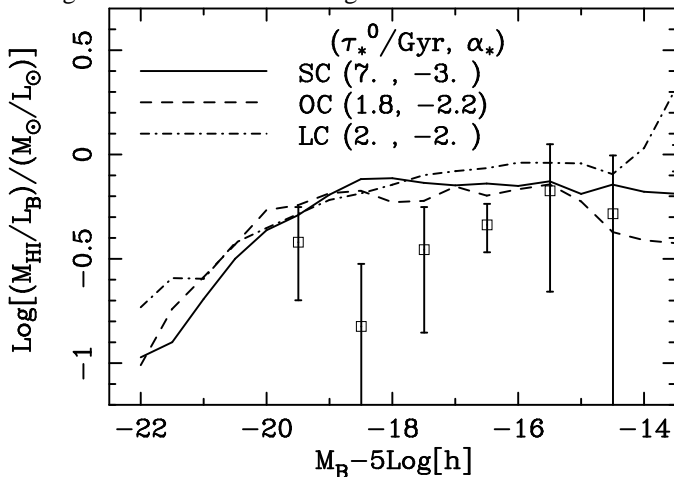


FIG. 4.— Cold gas mass relative to B -band luminosity of spiral galaxies. The solid, dashed, and dot-dashed curves show the SC, OC, and LC models, respectively. The open squares indicate the observational data for atomic neutral hydrogen taken from Huchtmeier & Richter (1988). In the models the cold gas consists of all species of elements, therefore its mass is multiplied by 0.75, i.e., $M_{\text{HI}} = 0.75M_{\text{cold}}$, which corresponds to the fraction of hydrogen. Because the observational data denote only atomic hydrogen, they should be regarded as lower limits of the ratio.

4. RESULTS

4.1. Galaxy Number Counts

Figure 5 shows the galaxy number counts in the Subaru K' -band as a function of apparent isophotal K' magnitude for the models of SC, OC, and LC. Thick lines show theoretical predictions based on the observational conditions, including the selection effects from the cosmological dimming of surface bright-

ness and completeness for galaxies in the SDF. Open circles indicate the observed SDF raw counts in isophotal magnitude. The number of galaxies in the SC model is too small to explain the observed raw counts (open circles with error bars). On the other hand, the OC and LC models explain the SDF counts equally well. For reference, the data from other surveys are also shown by the specified symbols, after applying a transformation of $K' = K + 0.1$.

Thin lines in this figure are theoretical predictions without the selection effects. It is evident that the effects become important at $K' > 20$, and make the count slope turn over at $K' \sim 24$, where the observed raw counts reach a maximum. The predicted counts with and without the selection effects differ by a factor of three at $K' \sim 24$, which is much greater than the observational error. Thus, incorporation of the selection effects is essential in the SAM analysis of the galaxy number counts.

We check for consistency with the HDF counts in the $UBVI$ bands in Figure 6. The types of lines are the same as in Figure 5. We see that the OC and LC models, which reproduce the near-infrared SDF counts, give a better agreement with the UV/optical HDF counts when compared with our previous models in NTGY. On the other hand, the SC model significantly falls below those observed in all the $UBVIK'$ bands. Thus we conclude that our SAMs well reproduce the multiband galaxy number counts in a low-density universes with or without a cosmological constant.

4.2. Isophotal Area-Magnitude Relation

As stressed in the previous section and in NTGY, the selection effects from the cosmological dimming of surface brightness of galaxies cannot be ignored in the SAM analysis of galaxy number counts. This indicates that the size of high-redshift galaxies must be modeled properly. Figure 7 plots the SDF galaxies in the isophotal area-magnitude diagram. The data plotted are those for the SDF galaxies that are detected in both the K' and J bands. Only the LC model is shown, with various values of $\rho = 0$ (solid line), 0.5 (dashed line), and 1 (dot-dashed line), because other parameters involving the adopted cosmology and dust extinction hardly affect the result. The isophotal area becomes smaller for fainter apparent magnitude; at faint limits it reaches the minimum for detection. All predictions with $\rho = 0-1$ give a convergent result at faint limit of $K' \sim 24$. This convergence occurs because galaxies with larger areas at $K' \sim 24$ have surface brightnesses below the threshold and remain undetected. We find from this figure that our SAM galaxies well reproduce the observed area-magnitude relation, and are consistent with the SDF galaxies, only when the selection bias against faint galaxies with high redshift and/or low surface brightness is taken into account in the analysis.

4.3. Redshift Distributions

The left panels in Figure 8 show the redshift distributions for the HDF galaxies in the I_{814} band. The solid and dashed lines are theoretical predictions for the LC model with and without the selection effects, respectively. The histograms are the observed photometric redshift distributions given by Furusawa et al. (2000). As shown in NTGY, the LC model well reproduces the observed redshift distribution as a function of apparent magnitude.

The right panels of Figure 8 show the K' -band predictions for the LC model. Compared with Totani et al. (2001a), in which the traditional models of galaxy evolution are used, the peak

location for our redshift distribution moves to lower redshift. Therefore, redshifts of the SDF galaxies, if measured by either a spectroscopic or photometric method, give an important insight into physical processes of galaxy formation and evolution.

5. MODEL UNCERTAINTIES AT HIGH REDSHIFT

In this section we discuss uncertainties in predicting the number counts of galaxies. Such uncertainties arise mainly from the SF timescale (§5.1), the galaxy size (§5.2), and the dust extinction (§5.3). As for the SN feedback-related parameters, we find that the dependence of our result on their values has a similar tendency to NTGY, so that our conclusion of preferring a low-density universe is not altered by uncertainty associated with these parameters. Finally we will discuss the morphological counts (§5.4).

5.1. Star Formation Timescale

We evaluate the effects of changing the SF timescale from CSF to DSF ($\sigma = 0$ or 1) in the Λ CDM model (see equation 1). Note that CSF in the EdS universe is equivalent to DSF with $\sigma = 1.5$, thus the case of DSF with $\sigma = 1$ is in between CSF and DSF with $\sigma = 0$, as shown in Figure 1. Hereafter, the two cases of DSF with $\sigma = 0$ and 1 in the Λ CDM model are referred to as LD0 and LD1, respectively.

Figure 9 shows the predicted number counts of galaxies in the Subaru K' and *HST* B_{450} bands for the models of LC (solid line), LD1 (dashed line) and LD0 (dot-dashed line). The predicted counts from LD1 and LD0 are higher than those by LC; this tendency is much more prominent in the longer wavelength passband. This wavelength-dependent tendency is explained as follows. In general, the near-infrared luminosity in the K' band mainly reflects the total mass of long-lived stars, while the UV/blue luminosity reflects the instantaneous SFR. While the total mass of cold gas available for star formation is limited by the radiative cooling of hot gas, the conversion timescale from cold gas to stars is determined by the SF timescale. In the case of DSF, for which the SF timescale is shorter than in CSF, more stars are formed at higher redshift. Consequently, in the cases of LD1 and LD0, individual galaxies become brighter in the K' band, and so the K' -band counts of observable galaxies above the surface brightness threshold become larger than in LC, although their blue luminosity is hardly changed in the B_{450} band.

The above argument indicates that the SF timescale is best constrained by the observed SDF counts in the K' band. Since the LC model is found to give a superior agreement with the SDF counts, the SF timescale should therefore be nearly constant against redshift. This result is consistent with previous SAM analyses by Kauffmann & Haehnelt (2000), Somerville, Primack & Faber (2001) and NTGY.

The optical depth for absorption of stellar light by dust is assumed to be proportional to the amount of cold gas present. In the cases of LD1 and LD0, because of the short SF timescale, the fraction of cold gas mass at high redshift is smaller, leading to smaller optical depth when compared to LC. For this reason, the B_{450} -band counts in LD1 and LD0, which are sensitive to internal dust extinction, show a slight excess at $B_{450} \sim 23$. However this effect is almost canceled out by the increase of stars due to the higher SFR given by the shorter SF timescale, as shown in Figure 9b.

5.2. Galaxy Size

As mentioned in §4.1, the selection effects from the cosmological dimming of surface brightness of galaxies are important. Therefore, the number counts of galaxies are sensitive to their size, because the surface brightness is proportional to the inverse of radius squared. Figure 10 shows theoretical predictions for the LC model with $\rho = 0$ (solid line), 0.5 (dashed line), and 1 (dot-dashed line). Note that the simple model with $\rho = 0$ leads to smaller disk size at high redshift in proportional to the initial radius r_i , which is nearly equal to the virial radius in the case of halos with galactic mass-scale and becomes smaller size according to the spherical collapse model. Thus the models with $\rho > 0$ lead to larger disks and lower surface brightness compared to the simple model with $\rho = 0$, and hence the smaller number counts of observable galaxies above the surface brightness threshold, in both the K' and B_{450} bands, when compared to the standard case of $\rho = 0$. Since the case of $\rho = 0$ slightly overpredicts the K' -band observed counts at $K' \sim 24$ and the case of $\rho \sim 0.5$ is preferable, it seems that high-redshift galaxies might be more extended in size than expected from the cooling radius.

The size of a galaxy disk also affects dust extinction. The optical depth of dust is proportional to the inverse of disk radius squared. In the case of $\rho = 1$, the number of galaxies at $B_{450} \sim 23$ increases above the $\rho = 0$ prediction, because of weaker dust extinction owing to larger disk size. The effects of dust extinction are discussed in the next section in detail.

The physical processes which cause the galaxy disks to be more extended at high redshift are yet to be identified. One possibility includes the viscous evolution of the star-forming disk (Saio & Yoshii 1990), but more investigations will obviously be necessary here.

5.3. Dust Extinction

The uncertainty in estimation of dust extinction at high redshift comes from a combination of uncertainties in the chemical enrichment model, dust-to-metal ratio, clumpiness of dust, and so on. Instead of entering into these details, however, we measure a robustness of our result by changing the value of γ in the optical depth by dust (equation 3).

Figure 11 shows theoretical predictions for the LC model with $\gamma = 0$ (solid line), 1 (dashed line), and 2 (dot-dashed line), assuming the slab dust distribution. The predicted K' -band counts are almost independent of γ (Figure 11a) because the near-infrared passbands are insensitive to dust extinction. On the other hand, the predicted B_{450} -band counts are sensitive to dust extinction (Figure 11b). In the case of $\gamma \geq 1$, the “knee” in the count curve near $B_{450} \sim 24$ mag becomes prominent. It might be therefore necessary to adopt a high value of $\gamma \gtrsim 1$ in order to reproduce the observed B_{450} -band counts better over a wide range of B_{450} -magnitude if the simple assumption of disk size in the previous subsection is correct.

Figure 12 is the same as Figure 11, except for showing theoretical predictions for the screen dust distribution with $\gamma = 0$ (dashed line) and 2 (dot-dashed line), in comparison with the slab dust distribution with $\gamma = 0$ (solid line). In general, when the value of optical depth is fixed in the case of $\gamma = 0$, the screen dust model gives stronger extinction than the slab dust model, so that the predicted number of bright galaxies at $B_{450} \lesssim 23$ becomes only slightly lower than that for the slab dust. In the case of $\gamma = 2$, the “knee” in the count curve near $B_{450} \sim 24$ mag is prominent even in the screen dust model. On the other hand, the predicted K' -band counts are not affected at all, and are there-

fore free from the uncertainty in estimation of dust extinction.

The most effective discriminator of dust extinction is the knee of observed galaxy counts at $B_{450} \sim 23$. When the dust extinction is strong, the knee disappears and the count curve deviates below the data. Therefore, the optical depth by dust should be small at high redshift, that is, $z \gtrsim 1$. We find that the knee is sensitive almost exclusively to the optical depth, which is determined by the cold gas mass, disk size, metallicity of cold gas, and γ (equation [3]).

In order to decrease the optical depth we need to decrease the cold gas mass and/or metallicity, expand the galaxy size, or increase the value of γ . If one decreases the cold gas mass with a shorter SF timescale, too many galaxies are formed, and the number of galaxies in the K' -band is overpredicted (§5.1). If one expands the galaxy size, we suffer from too strong selection effects (§5.2). There is an uncertainty in estimation of the cold gas metallicity (Somerville, Primack & Faber 2001), but this uncertainty can be practically absorbed in the effect of γ . Thus, in the usual SAMs ($\gamma = 0$), a simple estimation of optical depth might be worse to reproduce the observed galaxy counts at short wavelengths rather than models with a high value of $\gamma \gtrsim 1$. In any case, the shape of galaxy counts at shorter wavelength is sensitive to the optical depth. We will need more investigations on the dust extinction.

5.4. Morphology-Dependent Number Counts

Our SAM simultaneously reproduces the multi-band galaxy counts, in contrast to the previous works using the traditional galaxy evolution models (Totani & Yoshii 2000; Totani et al. 2001a). The reasons could indeed be quite complicated, but one of the possibilities might be that a dominant morphology of galaxies is different in different passband. The SAM allows for morphological transformations during the evolution of galaxies, that is, mergers between galaxies of similar mass make spheroidals as merger remnants, then they accrete hot gas through radiative cooling as galactic disk.

Figure 13 shows the predicted contributions of early-type galaxies (E/S0; dashed lines) in the LC model in the K' and I_{814} bands. Note that the morphology of galaxies is identified by the B -band bulge-to-disk ratio at their observed redshift in the observer frame and that this definition is different from that in usual analyses with the traditional models. The total number counts are also shown by the solid lines. In order to see the fractional change of morphologies, we change the value of f_{bulge} which divides mergers into major and minor ones according to the mass ratio of merging galaxies (see §2.1). The thick lines are for the reference value of $f_{\text{bulge}} = 0.1$, and the thin lines for $f_{\text{bulge}} = 0.5$ where major merger occurs only when the mass of smaller satellite is larger than 0.5 times that of larger one. We also plot the observed E/S0 counts in the HDF (Abraham et al. 1996; Driver et al. 1998; Phillipps et al. 2000) with the total HDF counts in the I_{814} -band. We find that our prediction for E/S0 counts roughly agree with the observed data and that the uncertainty in the E/S0 counts caused by that of f_{bulge} is nearly a factor of two.

We note that while the fraction of early-type galaxies increases with decreasing f_{bulge} , the total counts are hardly changed. This indicates that the total number of galaxies is essentially determined by the merging histories of dark halos and by the cooling rate of hot gas, and that the cooling must be very efficient to enable frequent formation of disk galaxies at $z \gtrsim 1$.

We also note that our morphological classification is based

on the B -band bulge-to-disk ratio. It has not yet been confirmed that this B -band classification coincides with that for the K' band, therefore our predictions of type-dependent counts in the K' band should be regarded as qualitative estimates.

6. SUMMARY AND DISCUSSION

We have calculated the number counts of faint galaxies in the framework of SAM for three cosmological models, the standard CDM (EdS) universe, a low-density open universe, and a low-density flat universe with nonzero Λ . Our SAM includes the selection effects from the cosmological dimming of surface brightness of galaxies with criteria appropriate for the SDF and HDF, and also includes some modifications to our previous analysis (NTGY), such as the optical depth estimation of dust within a galaxy. In this paper we have shown that our SAM is fully consistent with that of the previous version, and can explain the observed multi-band galaxy counts from the UV to the near-infrared.

Comparison of theoretical predictions with the observed number counts of SDF and HDF galaxies, as well as with other ground-based observations, indicates that the standard CDM is ruled out, and a Λ -dominated flat universe and a low-density open universe are favored. This result is consistent with that from HDF galaxies (NTGY), but is in sharp contrast with previous SAM analyses by other authors, where many of the conceivable selection effects in the faint observations have been ignored.

Some uncertainties in our SAM have been discussed. These arise from a lack of knowledge on the galaxy formation process, and also from an insufficient survey of the physical properties of high-redshift galaxies. We especially focused on the uncertainties in redshift dependence of SF timescale, galaxy size, and dust extinction. We found that dust extinction hardly affects galaxy counts in the Subaru K' band, but does significantly affect those in the $HST B_{450}$ band. Thus, the K' -band galaxy counts are robust against the uncertainty of dust extinction. Two other factors affect galaxy counts even in the K' -band. If the SF timescale at high redshift is shorter than one which is simply proportional to the dynamical timescale in the disk, too many galaxies are formed, and the number of galaxies at faint-end is greatly overpredicted. We found that the SF timescale should be nearly constant against redshift, as suggested by our previous analysis (NTGY) and by other recent SAM analyses (Kauffmann & Haehnelt 2000; Somerville, Primack & Faber 2001).

The uncertainty in estimation of galaxy size results in an uncertainty in estimation of the surface brightnesses of galaxies, which is directly related to the selection effects mentioned above. In our SAM, like usual SAMs, the size of the disk is determined under the assumption of specific angular momentum conservation of cooling gas, so that the disk size is proportional to the cooling radius. In order to see how theoretical predictions are changed by changing the galaxy size, we introduced a free parameter ρ allowing for an additional redshift dependence in size estimation. We found that the value of $\rho \gtrsim 0.5$ is favored in order to reproduce the observed counts, which indicates that the disk radius should be extended by a factor of $(1+z)$ over the cooling radius. We also found that this manipulation cannot be discriminated observationally because we cannot know how many undetected low surface brightness galaxies below the selection criteria are there at high redshift, which are presumably systems of large size.

Through this work, we have shown that our SAM can explain a variety of observed properties of nearby and high-redshift galaxies, and place some constraints on star formation, size evolution, and dust extinction. More stringent constraints will certainly be obtained by a greater knowledge of dynamical and kinematical properties of galaxies in near future.

We would like to thank T. C. Beers for his critical reading of the manuscript and T. Kodama for kindly giving us the data

of the pass-bands in the SDF. We also thank the anonymous referee who led us to a improvement of our paper. This work has been supported in part by the Grant-in-Aid for the Center-of-Excellence research (07CE2002) and for the Scientific Research Funds (13640249 and 12047233) of the Ministry of Education, Science, Sports and Culture of Japan. Numerical computation in this work was partly carried out at the Yukawa Institute Computer Facility.

REFERENCES

- Abraham, R.G., Tanvir, N.R., Santiago, B.X., Ellis, R.S., Glazebrook, K., & van den Bergh, S. 1996, *MNRAS*, 279, 47
- Arimoto, N., & Yoshii, Y. 1986, *A&A*, 164, 260
- Arimoto, N., & Yoshii, Y. 1987, *A&A*, 173, 23
- Arimoto, N., Yoshii, Y., & Takahara, F. 1991, *A&A*, 253, 21
- Baugh, C. M., Cole, S., & Frenk, C. S. 1996, *MNRAS*, 283, 1361
- Baugh, C. M., Cole, S., Frenk, C. S., & Lacey, C. G. 1998, *ApJ*, 498, 504
- Binney, J., & Tremaine, S. 1987, *Galactic Dynamics*, Princeton Univ. Press, Princeton, NJ
- Blanton, M.R. et al. 2001, *AJ*, 121, 2358
- Bond, J. R., Cole, S., Efstathiou, G., & Kaiser, N. 1991, *ApJ*, 379, 440
- Bower, R. 1991, *MNRAS*, 248, 332
- Catelan, P., & Theuns, T. 1996a, *MNRAS*, 282, 436
- Catelan, P., & Theuns, T. 1996b, *MNRAS*, 282, 455
- Cole, S., Aragon-Salamanca, A., Frenk, C. S., Navarro, J. F., & Zepf, S. E. 1994, *MNRAS*, 271, 781
- Cole, S., Lacey, C. G., Baugh, C. M., & Frenk, C. S. 2000, *MNRAS*, 319, 168
- Cole, S. et al. 2001, *MNRAS*, 326, 255
- Driver, S.P., Fernández-Soto, A., Couch, W.J., Odewahn, S.C., Windhorst, R.A., Phillipps, S., Lanzetta, K., & Yahil, A. 1998, *ApJ*, 496, 93
- Eke, V. R., Cole, S., & Frenk, C. S. 1996, *MNRAS*, 282, 263
- Fall, S. M. 1979, *Nature*, 281, 200
- Fall, S. M., & Efstathiou, G. 1980, *MNRAS*, 193, 189
- Fall, S. M. 1983, in 'Internal kinematics and dynamics of galaxies', proceedings of the IAU symposium 100, Besancon, France, Dordrecht, D. Reidel, p.391
- Fernández-Soto, A., Lanzetta, K. M., & Yahil, A. 1999, *ApJ*, 513, 34
- Folkes, S. et al. 1999, *MNRAS*, 308, 459
- Furusawa, H., Shimasaku, K., Doi, M., & Okamura, S. 2000, *ApJ*, 534, 624
- Gardner, J. P., Sharples, R. M., Carrasco, B. E., & Frenk, C. S. 1996, *MNRAS*, 282, L1
- Gardner, J. P., Sharples, R. M., Frenk, C. S., & Carrasco, B. E. 1997, *ApJ*, 480, L99
- Glazebrook, K., Peacock, J.A., Miller, L., & Collins, C.A. 1994, *MNRAS*, 266, 65
- Gunn, J.E., & Gott, J.R. 1972, *ApJ*, 176, 1
- Hall, P., & Mackay, C. B. 1984, *MNRAS*, 210, 979
- Heyl, J. S., Cole, S., Frenk, C. S., & Navarro, J. F. 1995, *MNRAS*, 274, 755
- Huchtmeier, W. K., & Richter, O. -G. 1988, *A&A*, 203, 237
- Impey, C.D., Sprayberry, D., Irwin, M. J., & Bothun, G. D. 1996, *ApJS*, 105, 209
- Jones, L.R., Fong, R., Shanks, T., Ellis, R. S., & Peterson, B. A. 1991, *MNRAS*, 249, 481
- Kauffmann, G., & Haehnelt, M. 2000, *MNRAS*, 311, 576
- Kauffmann, G., White, S. D. M., & Guiderdoni, B. 1993, *MNRAS*, 264, 201
- Kauffmann, G., Guiderdoni, B., & White, S. D. M. 1993, *MNRAS*, 267, 981
- Kodama, T., & Arimoto, N. 1997, *A&A*, 320, 41
- Koo, D.C. 1986, *ApJ*, 311, 651
- Lacey, C.G., & Cole, S. 1993, *MNRAS*, 262, 627
- Lanzetta, K.M., Yahata, N., Pascarelle, S., Chen, H.-W., & Fernández-Soto, A. 2002, preprint, astro-ph/0111129
- Loveday, J., Peterson, B. A., Efstathiou, G., & Maddox, S. J. 1992, *ApJ*, 90, 338
- Maddox, S. J., Sutherland, W. J., Efstathiou, G., Loveday, J., & Peterson, B. A. 1990, *MNRAS*, 247, 1p
- Maihara, T. et al. 2001, *PASJ*, 53, 25
- Makino, J., & Hut, P. 1997, *ApJ*, 481, 83
- McLeod, B.A., Bernstein, G.M., Rieke, M.J., Tollestrup, E.V., & Fazio, G.G. 1995, *ApJS*, 96, 117
- Metcalfe, N., Shanks, T., Fong, R., & Jones, L. R. 1991, *MNRAS*, 249, 498
- Minezaki, T., Kobayashi, Y., Yoshii, Y., & Peterson, B.A. 1998, *ApJ*, 494, 111
- Mo, H.J., Mao, S., & White, S.D.M. 1998, *MNRAS*, 295, 319
- Mobasher, B., Sharples, R. M., & Ellis, R. S. 1993, *MNRAS*, 263, 560
- Nagashima, M., & Gouda, N. 1997, *MNRAS*, 301, 849
- Nagashima, M., Totani, T., Gouda, N., & Yoshii, Y. 2001, *ApJ*, 557, 505 (NTGY)
- Netterfield, C. B. et al. 2001, preprint, astro-ph/0104460
- Peebles, P. J. E. 1993, *Principles of Physical Cosmology*, Princeton Univ. Press, Princeton, NJ
- Phillipps, S., Driver, S.P., Couch, W.J., Fernández-Soto, A., Bristow, P.D., Odewahn, S.C., Windhorst, R.A., & Lanzetta, K. 2000, *MNRAS*, 319, 807
- Press, W., & Schechter, P. 1974, *ApJ*, 187, 425
- Ratcliffe, A., Shanks, T., Parker, Q., & Fong, R. 1998, *MNRAS*, 293, 197
- Saio, H., & Yoshii, Y. 1990, *ApJ*, 363, 40
- Simien, F., & de Vaucouleurs, G. 1986, *ApJ*, 302, 564
- Somerville, R.S., & Kolatt, T. 1999, *MNRAS*, 305, 1
- Somerville, R.S., & Primack, J. R. 1999, *MNRAS*, 310, 1087
- Somerville, R.S., Primack, J. R., & Faber, S. M. 2001, *MNRAS*, 320, 504
- Sutherland, R., & Dopita, M. A. 1993, *ApJS*, 88, 253
- Suzuki, T.K., Yoshii, Y., & Beers, T.C. 2000, *ApJ*, 540, 99
- Tomita, K. 1969, *Prog. Theor. Phys.*, 42, 9
- Totani, T., & Yoshii, Y. 2000, *ApJ*, 540, 81
- Totani, T., Yoshii, Y., Maihara, T., Iwamuro, F., & Motohara, K. 2001a, *ApJ*, 559, 592
- Totani, T., Yoshii, Y., Iwamuro, F., Maihara, T., & Motohara, K. 2001b, *ApJ*, 558, L87
- Totani, T., & Takeuchi, T.T. 2002, *ApJ* in press (astro-ph/0201277)
- Tyson, J.A. 1988, *AJ*, 96, 1
- White, S.D.M. 1984, *ApJ*, 286, 38
- Williams, R. T. et al. 1996, *AJ*, 112, 1335
- Yoshii, Y. 1993, *ApJ*, 403, 552
- Yoshii, Y., & Arimoto, N. 1987, *A&A*, 188, 13
- Yoshii, Y., & Peterson, B. A. 1991, *ApJ*, 372, 8
- Yoshii, Y., & Peterson, B. A. 1994, *ApJ*, 436, 551
- Yoshii, Y., & Peterson, B. A. 1995, *ApJ*, 444, 15
- Yoshii, Y., & Takahara, F. 1988, *ApJ*, 326, 1
- Zucca, E. et al. 1997, *A&A*, 326, 477

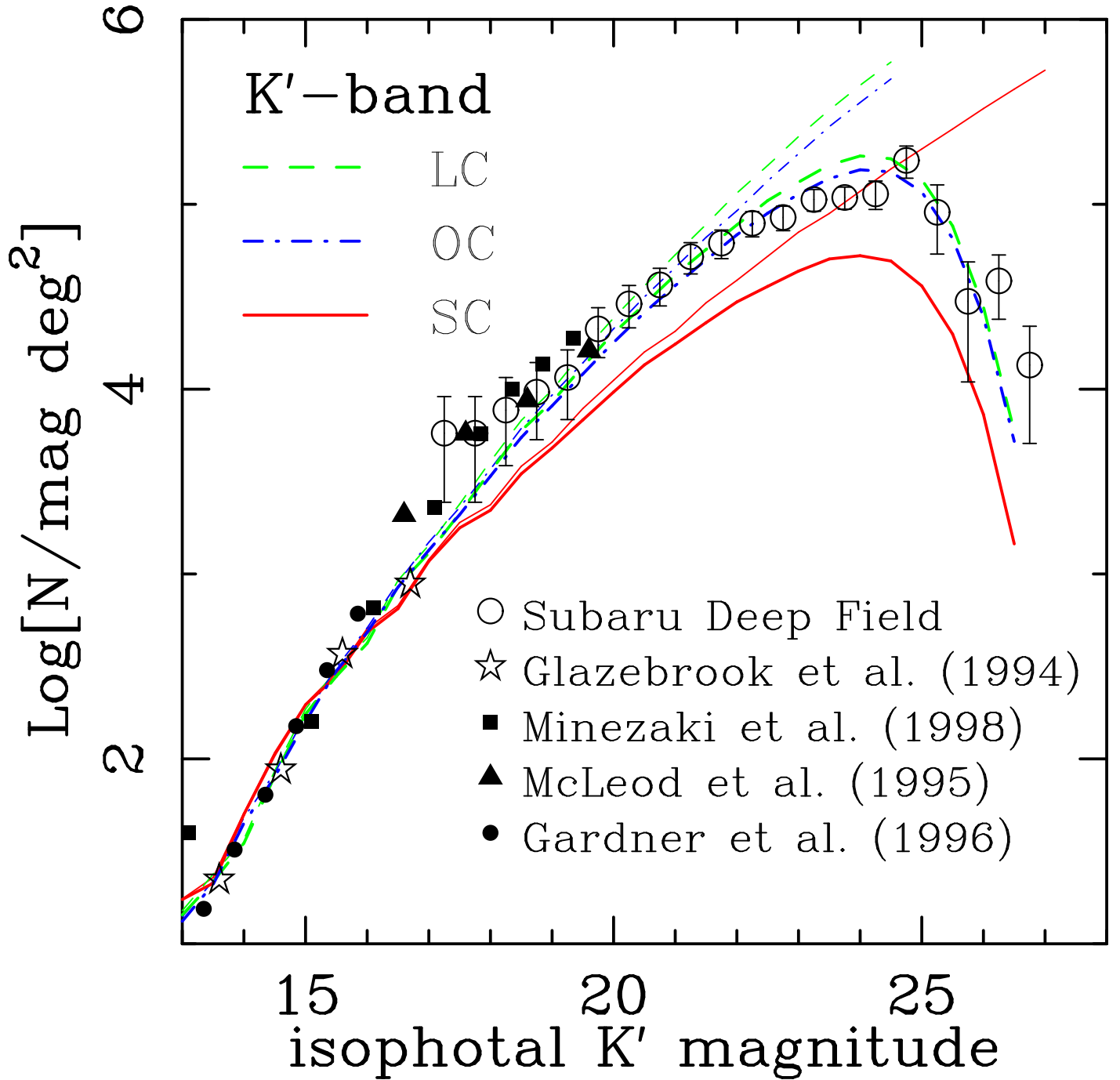


FIG. 5. — Number-magnitude relations for various cosmological models in the Subaru K' -band. The solid, dot-dashed, and dashed lines indicate SC, OC, and LC, respectively. The thick lines denote the models including the selection effects, while the thin lines denote those without the selection effects. The open circles with errorbars indicate the raw counts in the SDF. The other symbols indicate other observational data referred in the figure.

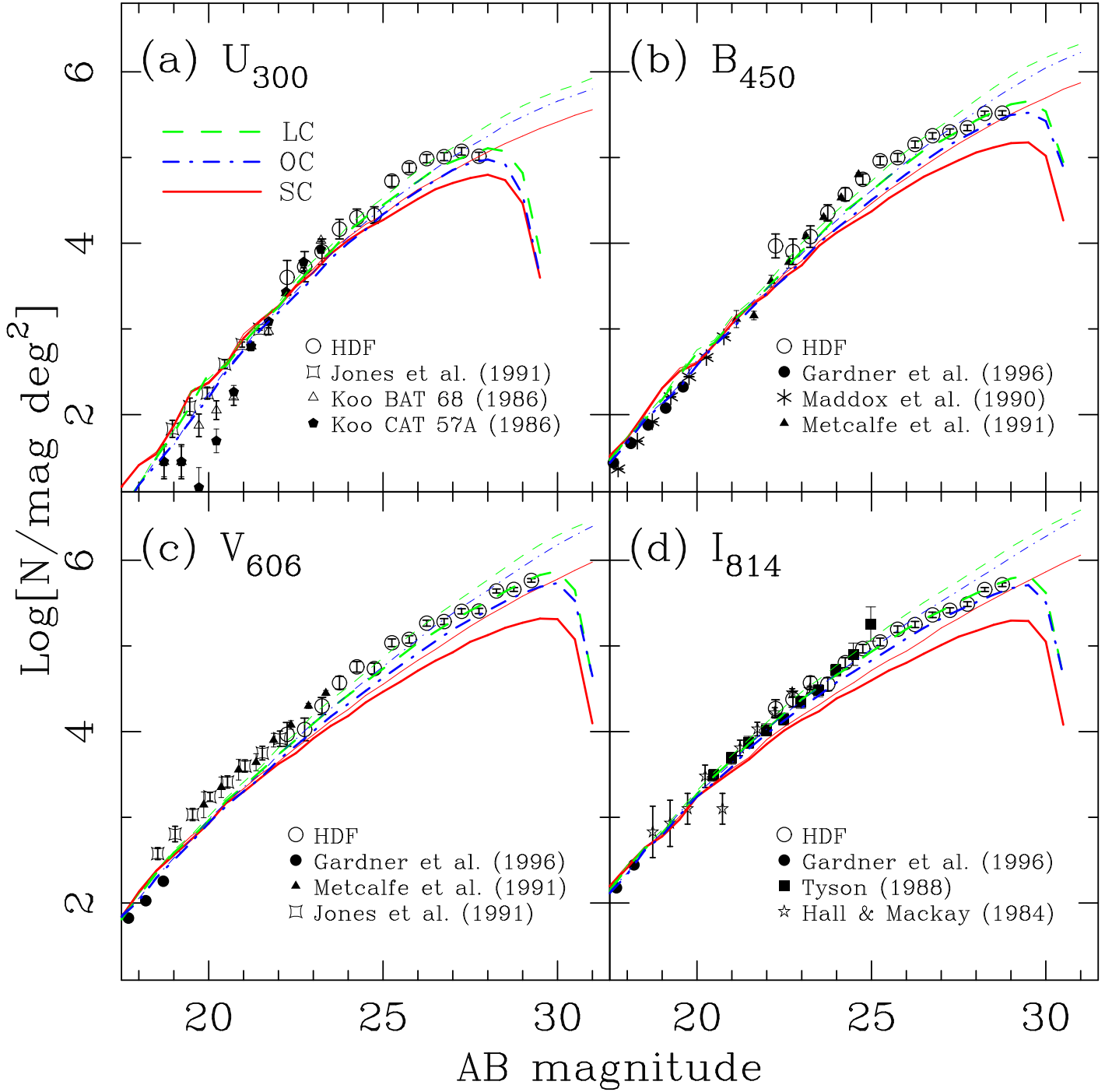


FIG. 6.— Number-magnitude relations for various cosmological models in the *HST* *UBVI*-bands. Types of lines are the same as Figure 5. The symbols indicate observational data referred to in the figure.

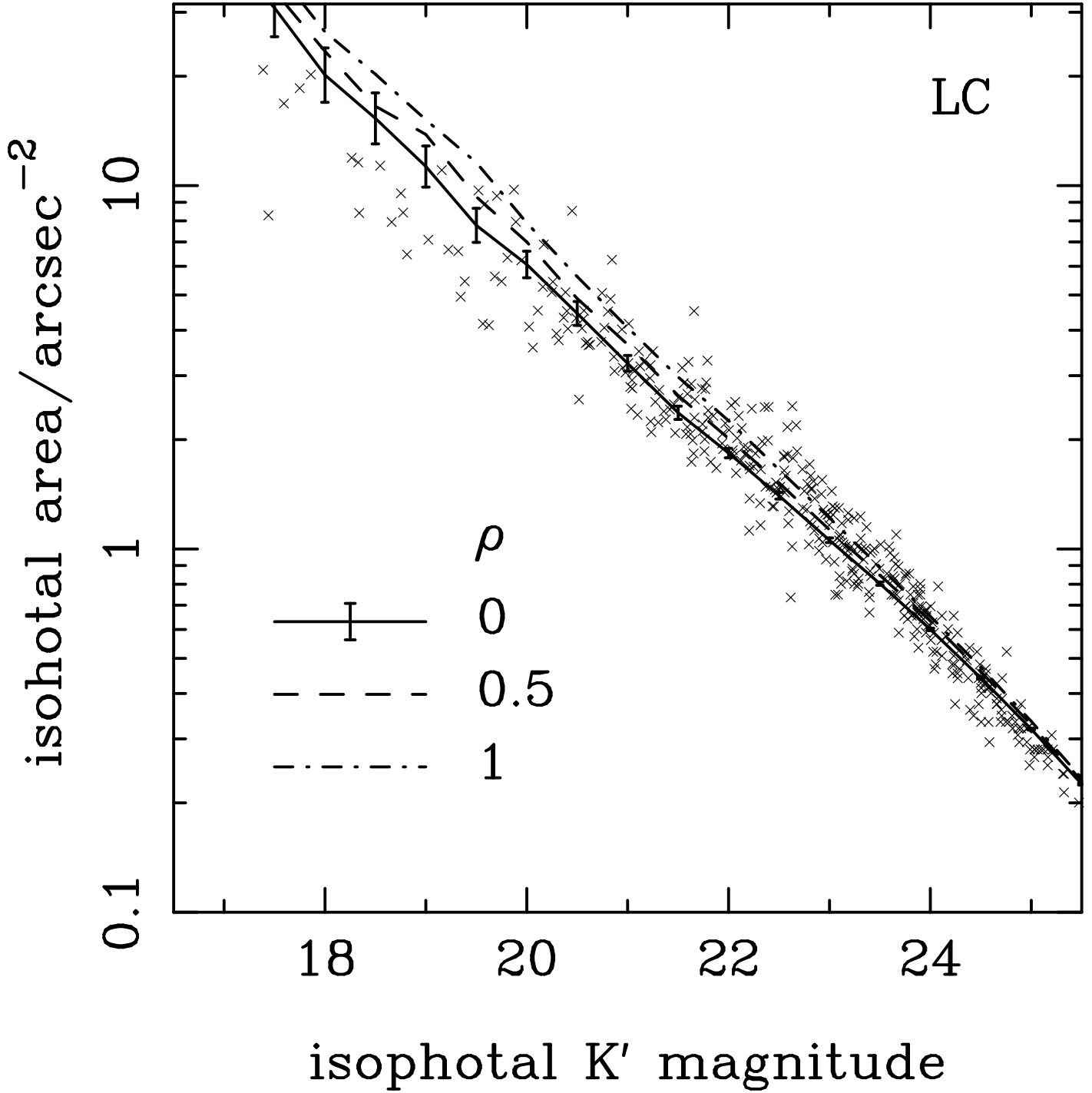


FIG. 7.— Isohotal area of galaxies detected in both the K' and J bands in the LC model. The parameter ρ is varied from 0 (solid line), via 0.5 (dashed line), to 1 (dot-dashed line). The 1σ scatters in the model with $\rho = 0$ are shown by error bars. The crosses indicate the data in the SDF.

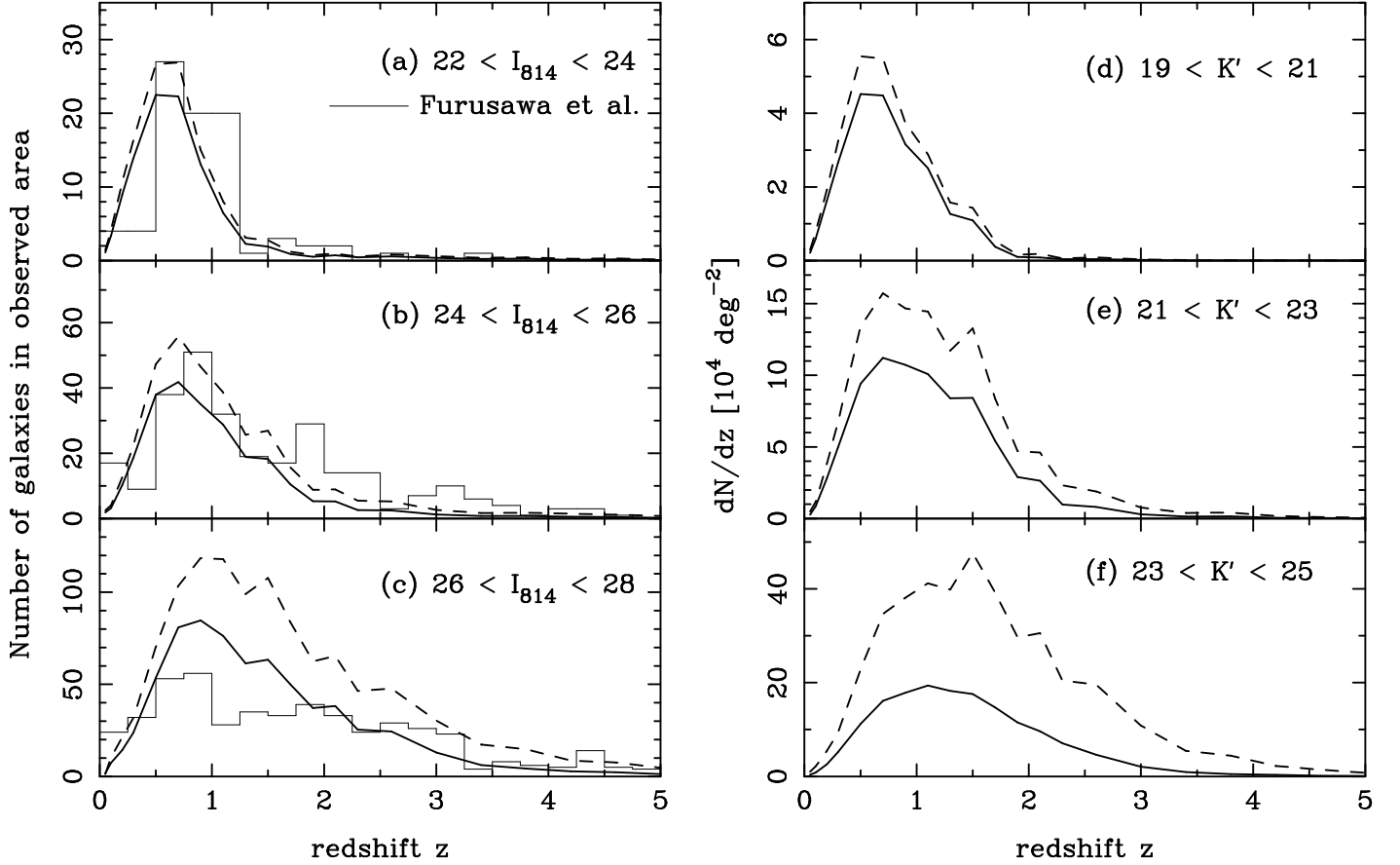


FIG. 8.— Redshift distributions of galaxies for a Λ -dominated flat CDM model. Left panels: the I_{814} -band. Right panels: the K' -band. The solid and dashed lines denote the LC model with and without the selection effects, respectively. The histograms in the left panels indicate the redshift distributions of the HDF galaxies derived by Furusawa et al. (2000), using an improved technique of photometric redshift estimation.

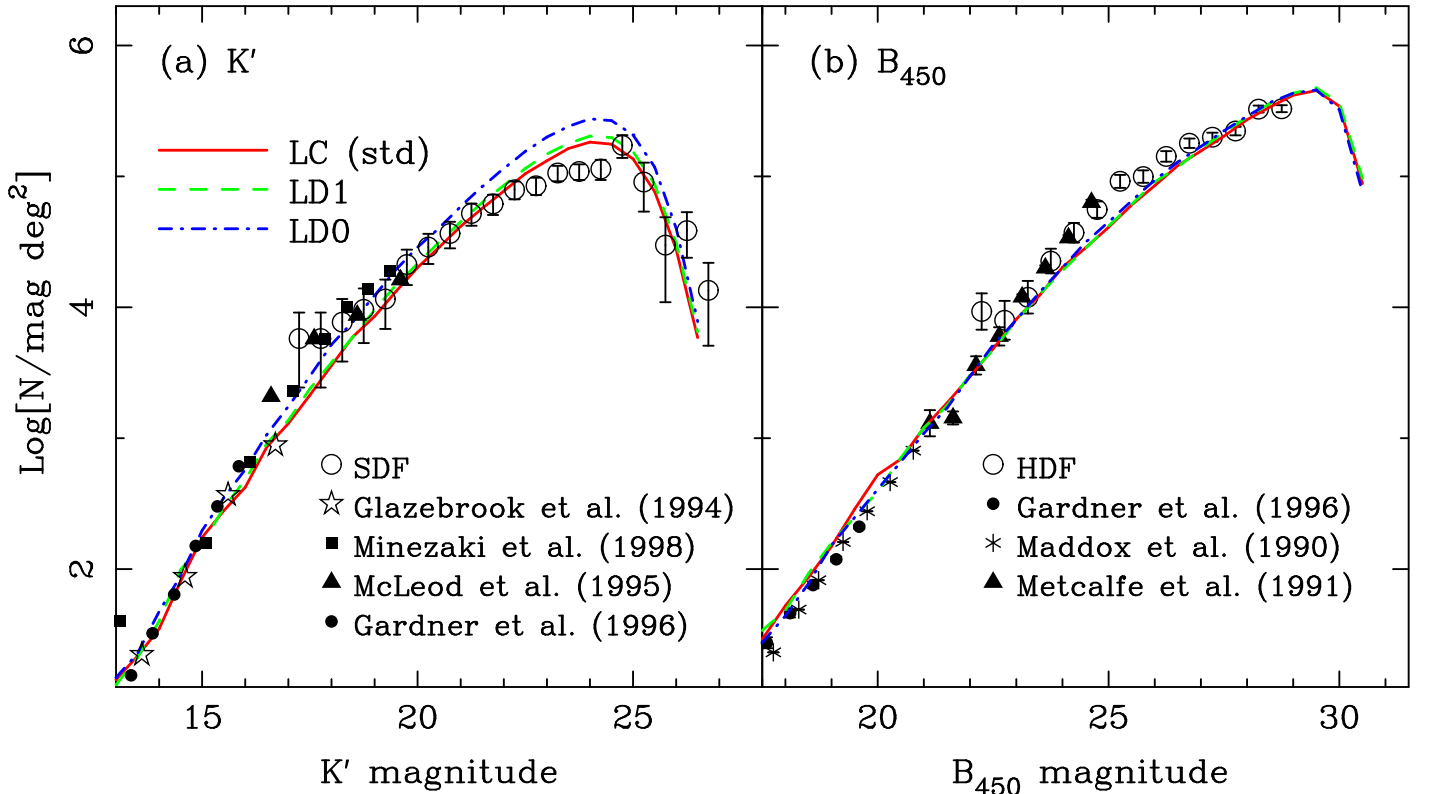


FIG. 9.— Number-magnitude relations for a Λ -dominated flat CDM model. The solid, dashed, and dot-dashed lines indicate the LC (CSF), LD1 (DSF with $\sigma = 1$), and LD0 (DSF with $\sigma = 1$) models, respectively.

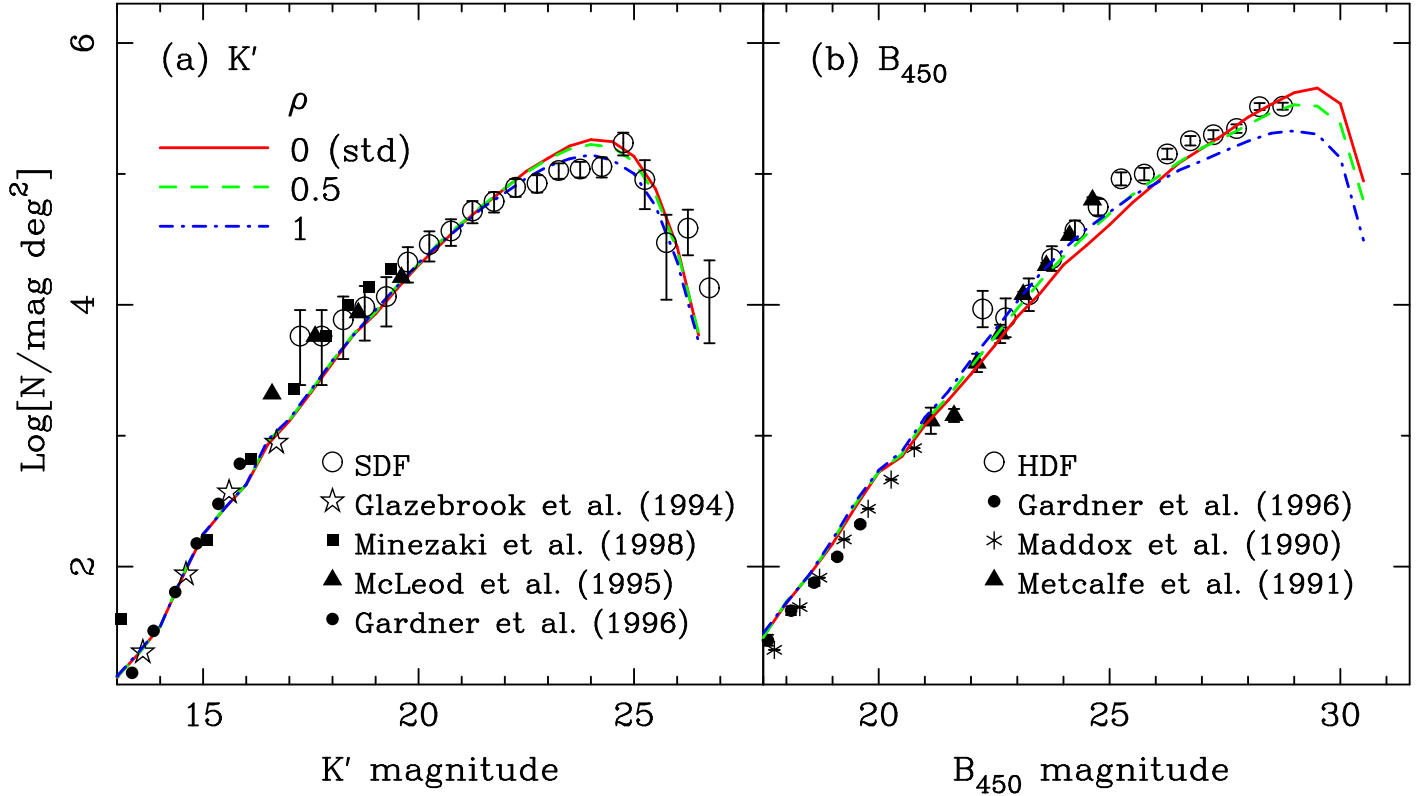


FIG. 10.— Number-magnitude relations for a Λ -dominated flat CDM model. The solid, dashed, and dot-dashed lines indicate the LC models with different z -dependences of galaxy size, $\rho = 0, 0.5,$ and 1 , respectively.

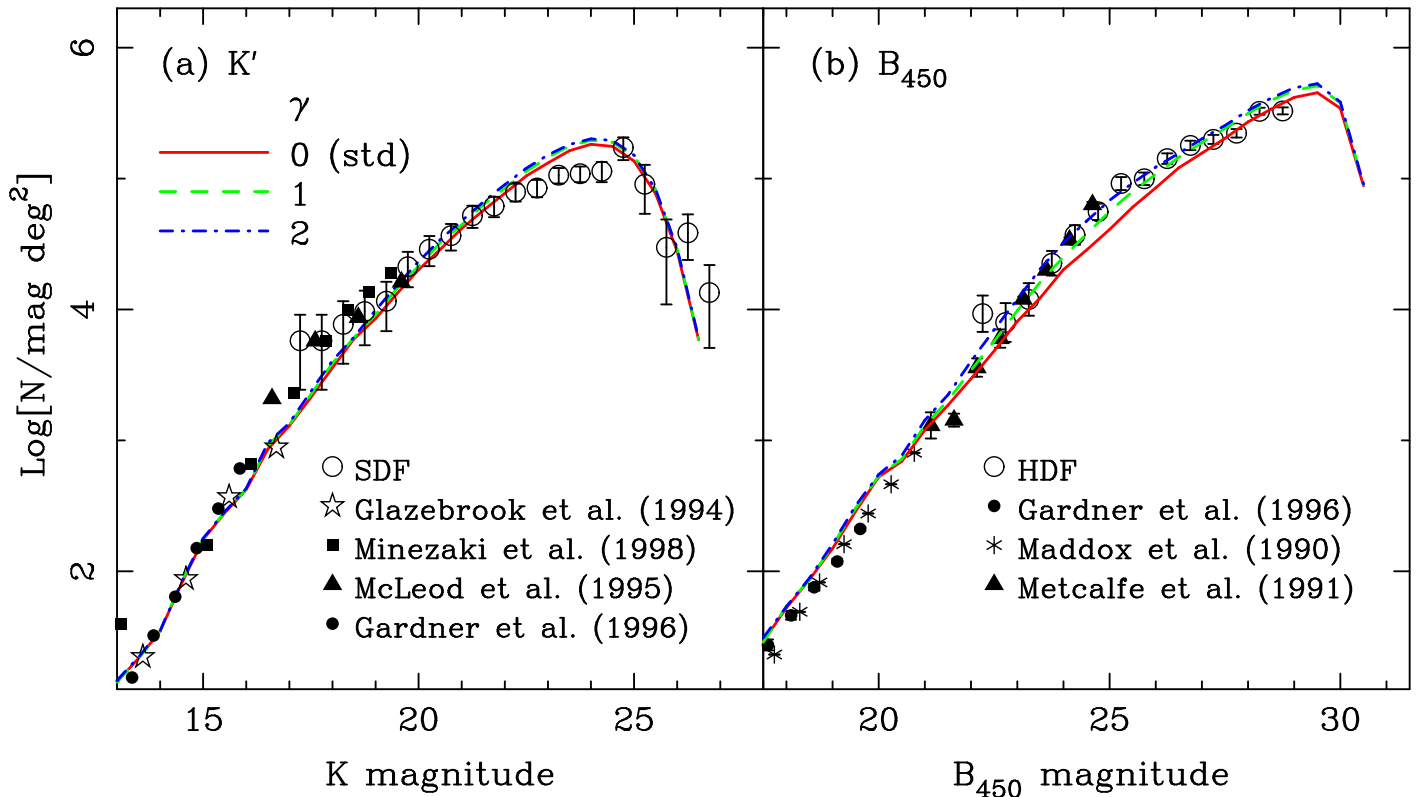


FIG. 11.— Number-magnitude relations for a Λ -dominated flat CDM model. The solid, dashed, and dot-dashed lines indicate the LC models with different z -dependences of dust optical depth, $\gamma = 0, 1,$ and 2 , respectively, of the slab dust model.

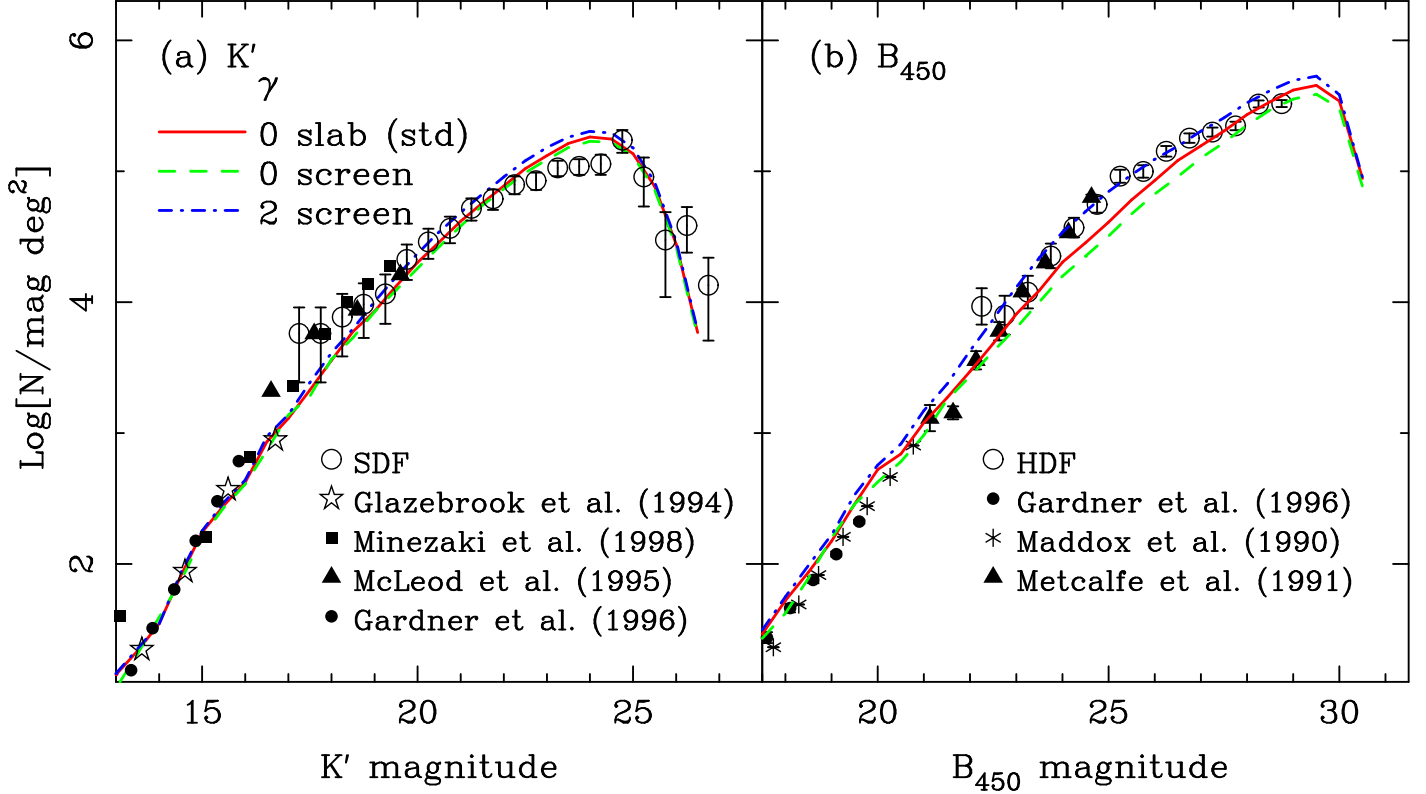


FIG. 12.— Number-magnitude relations for a Λ -dominated flat CDM model. The solid, dashed, and dot-dashed lines indicate the LC models with the *slab* dust with $\gamma = 0$, and the *screen* dust with $\gamma = 0$ and 2, respectively.

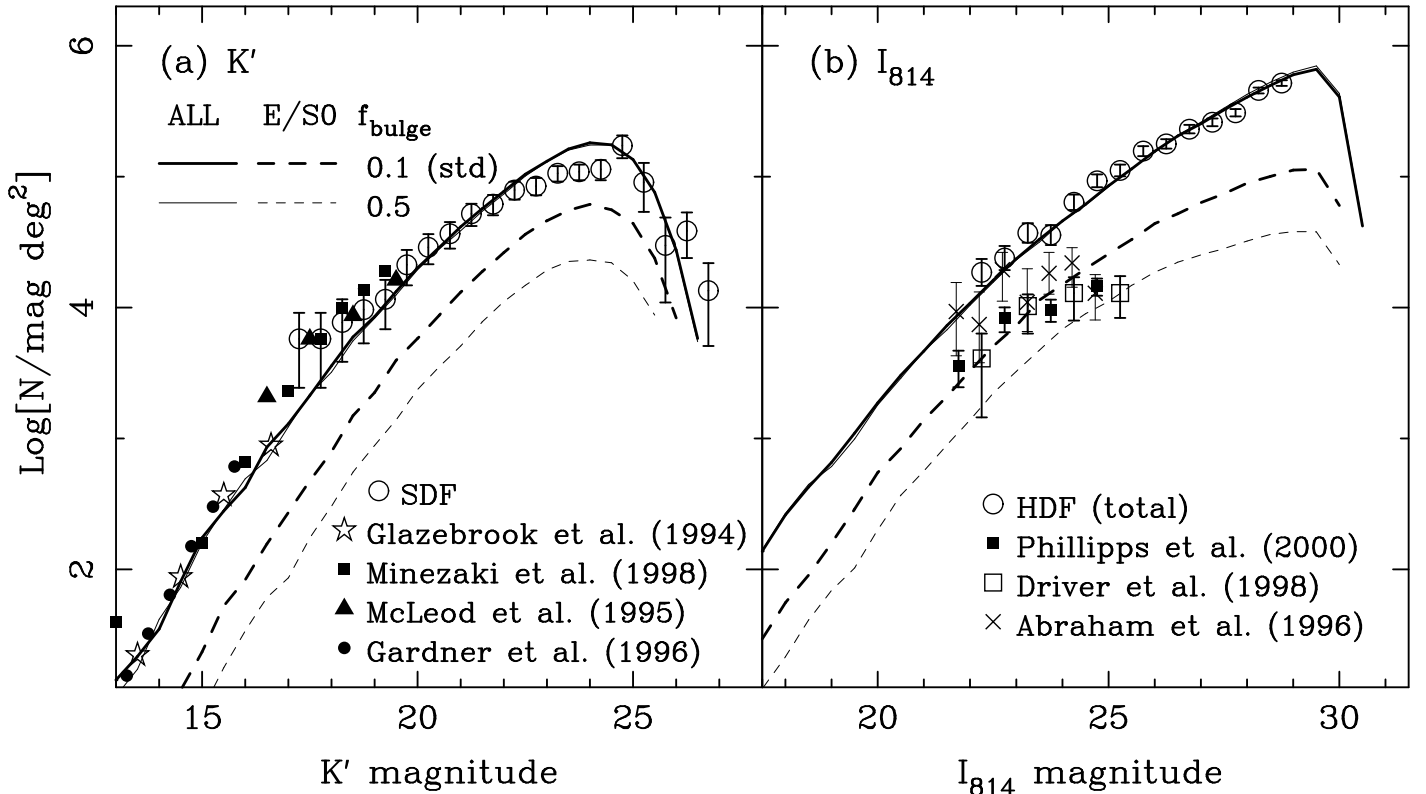


FIG. 13.— Morphology-dependent number-magnitude relations in the LC model. The solid and dashed lines indicate the total and early-type (E/S0) galaxy counts, respectively, in the LC model. The thick lines of these two are for $f_{\text{bulge}} = 0.1$, and the thin lines for $f_{\text{bulge}} = 0.5$ model.

TABLE 1
MODEL PARAMETERS

CDM Model	cosmological parameters				astrophysical parameters					
	Ω_b	Ω_Λ	h	σ_8	$V_{\text{hot}} \text{ (km s}^{-1}\text{)}$	α_{hot}	$\tau_*^0 \text{ (Gyr)}$	α_*	f_b	Υ
SC	1	0	0.5	0.67	350	5	7	-3	2	1
OC	0.3	0	0.6	1	240	3	1.8	-2.2	1	2
LC	0.3	0.7	0.7	1	280	2.5	2	-2	1	1.5

Note. — Equations defined the SN feedback-related parameters (V_{hot} and α_{hot}) and the SFR-related parameters (τ_*^0 and α_*) are (2) and (1), respectively. The definitions of last two parameters, f_b and Υ , are given in §§2.3 and 2.2, respectively. The other parameters used in common as standard include $\Omega_b = 0.015h^{-2}$, CSF (equation 1), $f_{\text{bulge}} = 0.1$ (§2.1), $\gamma = 0$ (equation 3), $\rho = 0$ (equation 6), and $(\bar{\lambda}, \sigma_\lambda) = (0.05, 0.5)$ (equation 5).